

Broadband Temporal Coherence Results From the June 2003 Panama City Coherence Experiments

H. Chandler*, E. Kennedy*, R. Meredith*, R. Goodman**, S. Stanic*

**Code 7184, Naval Research Laboratory Stennis Space Center, Ms. 39529.*

*** Department of Marine Sciences, University of Southern Mississippi
Stennis Space Center, Ms. 39529*

Abstract. During the month of June, 2003, the Naval Research Laboratory conducted a series of coherence experiments in shallow water (approximately 9 meters) off Panama City Beach, Florida. Examined here are preliminary mid frequency (1 - 10 kHz) results of analyzed temporal coherence data. For this experiment, a G34 omnidirectional source, mounted approximately 2.7 meters from the bottom, ensonified a vertical and horizontal array of hydrophones mounted on a submerged tower 70 and 150 meters down range in the along shore direction. Results will be shown for both macro (5 minutes), and micro events (<20 seconds).

INTRODUCTION

Temporal and spatial coherence of acoustic signals propagating in shallow water have a direct impact on the performance of Synthetic Aperture Sonar (SAS) and underwater communications systems. Causes of temporal coherence variability are numerous and are driven by oceanographic and meteorological dynamics which can include microstructure dynamics of the water column, sound speed variability, and boundary scattering. Even on relatively calm days, movement of the sea surface can present a randomly changing scattering surface. Volume scattering, either from biological scatterers, or, from entrained bubble plumes on rough days, can have a large effect on received signal amplitude and phase. In shallow waters, multipath interference compounds the effects of the dynamically changing waveguide. At present time, there is little experimental data available to adequately model these effects.

The objective of this paper is to present preliminary results of broadband temporal signal coherence from data obtained during the Panama City 2003 experiments. These measurements were conducted over a broad range of frequencies and changing oceanographic conditions over a relatively smooth, sandy bottom. There was no evidence of biological scatterers present during the examined runs. This paper will focus primarily on mid-frequency broadband results of 20 June 2003. These results represent the effects seen during a 10-minute period on a relatively calm day with an isovelocity water column, [1]. Coherence for the entire received signal is calculated i.e. no attempt has been made to resolve individual multipath arrivals; so the data have

not been match filtered. We also present some preliminary results of time of arrival fluctuations for these runs, and contrast them with results obtained on a stormy day.

EXPERIMENTAL CONFIGURATION

Figure 1 is a schematic representation of the experimental geometry. Broadband pulses were generated by a G34 projector 2.7 m above the ocean bottom. The G34 is a mid-frequency omnidirectional source having a bandwidth of 1 to 10 kHz and is capable of generating peak source levels of about 170 dB at 3.5 kHz. The source tower was deployed 545 m from the shoreline in a depth of approximately 8.8 m.

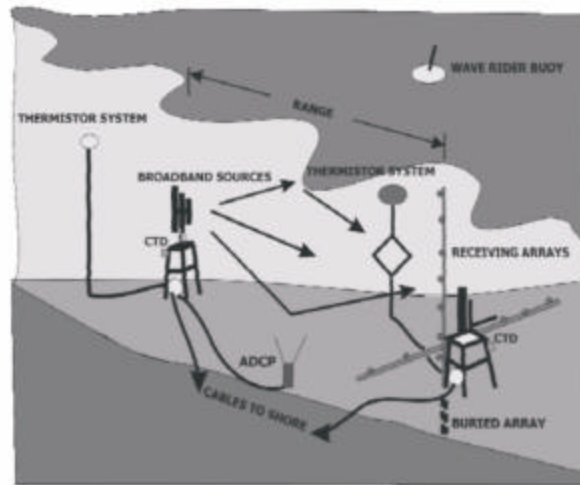


FIGURE 1. Experimental Layout.

Downrange, in a direction nearly parallel with the shoreline, a similar tower was deployed upon which were mounted various acoustic receiving arrays. These included a 12 m horizontal array with eight unequally spaced broadband hydrophones. This horizontal array was mounted on the tower 1.75 m above the bottom, and was orientated nearly perpendicular with the line of propagation from the source tower. Data were also collected on a 6 m vertical array of 10 equally spaced (0.53 m) low-frequency hydrophones but these data have not yet been examined. A complete description of the measurements, program objectives and experimental configuration is given in [2].

Figure 2 shows the low-frequency transmitted waveform and its spectrum. It is a 4 ms 1-10 kHz linear FM pulse equalized to compensate for the varying transmitting voltage response of the source transducer.

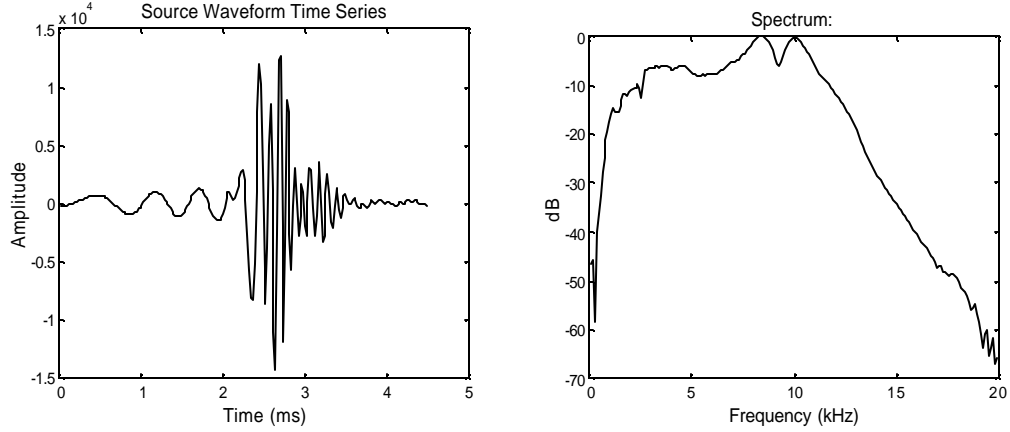


FIGURE 2. Time series and spectrum of the low-frequency source waveform

CALCULATING BROADBAND COHERENCE

For this experiment, pulses were transmitted at a rate of one per second, giving a temporal separation period (ΔT_p) of 1 second between pings. This allowed the comparison of signals separated in time by an integral number of time periods between pings (the temporal delay):

$$T_d = n\Delta T_p. \quad (1)$$

Source triggering and data collection were synchronized to a common clock so that each received pulse was digitally sampled within a 12 ms frame starting 46.6 ms after the commencement of acoustic transmission, with a sampling period. This yielded 800 to 1000 time aligned frames of received pings of 12 bit quantized hydrophone voltage,

$$E_i(m\Delta T_s), \quad m = 1, M \quad (2)$$

where $M = 1200$ samples, and i is the pulse number.

Broadband coherence in the time domain is defined in terms of the cross correlation function

$$C_{i,j}(\mathbf{t}) = \sum_{m=-M}^M E_i(\mathbf{t})E_j(m\Delta T_s + \mathbf{t}). \quad (3)$$

This term is then normalized to give a value of 1 for identical signals.

$$\mathbf{r}_{i,j}(\mathbf{t}) = \frac{C_{i,j}(\mathbf{t})}{\sqrt{C_{i,i}(0)C_{j,j}(0)}}. \quad (4)$$

Temporal coherence is given by the maximum value of the cross correlation function

$$\mathbf{j}_{i,j} = \left| \mathbf{r}_{i,j}(\mathbf{t}) \right|_{\max}. \quad (5)$$

For this study coherence as a function of time and temporal delay was examined for $n=1, 2, 3 \dots N$, for $N=20$ delays.

$$\mathbf{j}(t_i, T_d) = \left| \mathbf{r}_{i,i-n}(\mathbf{t}) \right|_{\max}, \quad n = 1, 2, 3, \dots, 20. \quad (6)$$

Figure 3 is a graphic illustration of how pulse pairs are selected for coherence processing. The dots represent the received pings on a particular hydrophone and are numbered in order of reception. The rows represent how pairs are selected for increasing temporal delay, T_d . For each n , a time series is formed. For example, on the first row, the first two dots are surrounded by a box to illustrate that adjacent pings are compared. This gives the first term in a time series. The box is then slid to the right one ping, and another comparison is made of adjacent pings. This process is repeated until the last ping is processed, and a time series is formed. The second row represents the case where the temporal delay between pings ($n\Delta T_p$) is 2 seconds and illustrates that the first comparison is made between the first ping and the ping $2\Delta T_p$ later. Again the box is slid to the right one ping and the second and 4th ping are compared, and so on to give a second time series.

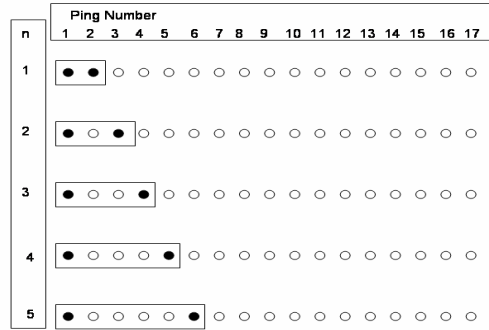


FIGURE 3. Coherence processing for temporal delay of 1 through 5 seconds

Figure 4 shows values of the ping-to-adjacent-ping ($n=1$) coherence as a function of time for all 8 hydrophones on the horizontal array for a calm day. During this 6.5 minute period, the temporal coherence seems to affect each channel in the array simultaneously. Though not illustrated, this apparent correlation of coherence

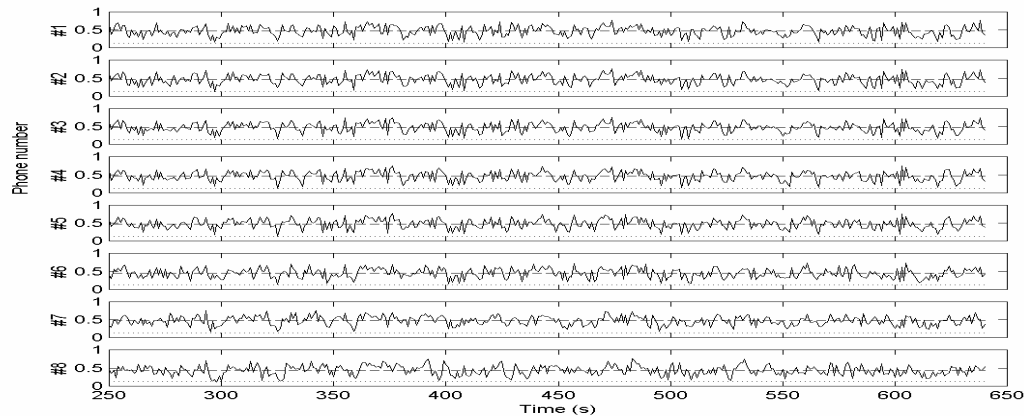


Figure 4. Temporal coherence vs. time for 1 second temporal delay

between hydrophones is evident for all delays processed. Figure 5 shows the mean coherence over the entire 6.5 minute period as a function of hydrophone. We find that there was little spatial dependence. Only hydrophone number 8 gave a somewhat lower coherence than the other hydrophones. Standard deviation is nearly constant at 0.14 across all phones.

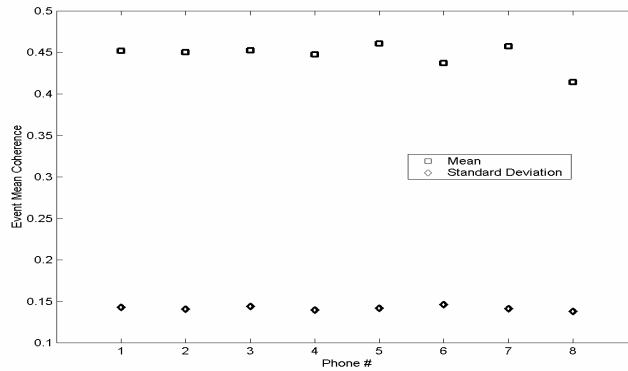


FIGURE 5. Mean coherence vs. hydrophone

Figure 6 shows the mean ping-to ping coherence of the entire 6.5 minute data set. each line represents a different hydrophone with the eighth hydrophone measuring somewhat lower the rest. In this figure we see that the coherence over the 6.5 minutes varies only slightly about the mean of around 0.45.

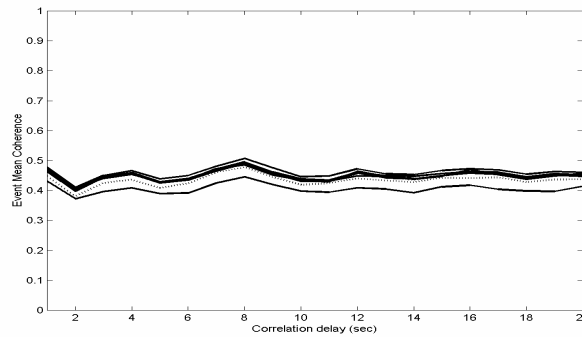


FIGURE 6. Mean coherence vs. temporal delay

Figure 7 shows the measured coherence, for $N = 20$ calculated temporal delays, as a function of time on a calm day (winds less than 10 knots) at a range of 70 meters. Twenty successive pings are shown, with each of the 20 lines representing one of the different temporal delay interval, $T_d = n\Delta T$, for $n = 1, 2, 3, \dots, 20$. We observe that coherence as a function of time and for all 20 T_d varies randomly about a central mean as shown by the solid line in Fig 8.

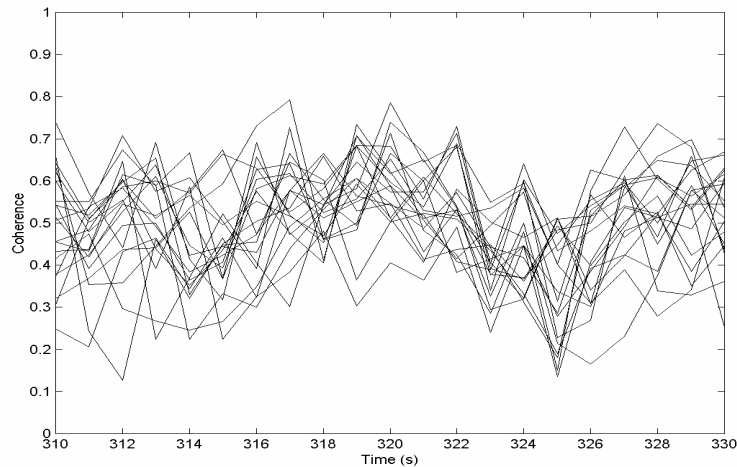


FIGURE 7. Coherence vs. time for all 20 computed temporal delays

The fluctuation of the mean as a function of time seems to be consistent with the swell period. Furthermore, Fig 8 shows that the standard deviation (dashed line below) of the individually computed temporal delays is nearly stationary for this 20-second period, with standard deviation of 0.11.

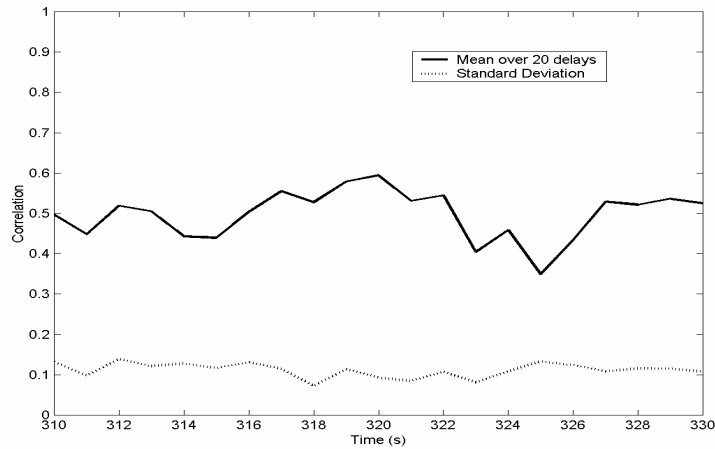


FIGURE 8. Mean and standard deviation of coherence over 20 pulses

AMPLITUDE AND TIME OF ARRIVAL FLUCTUATIONS

Table 1 summarizes the time of arrival for the first significant source-receiver propagation paths as calculated from a ray-trace model. The first bottom bounce arrives 256 μsec after the direct path. The surface multipath does not contaminate the received signal until 456 μsec after receiving the leading edge of the direct path arrival. Since both source and receiver are fixed, the first bottom bounce has no appreciable effect on temporal coherence. Therefore, measuring the fluctuations in the

time of arrival of the source waveform using the leading 450 μsec of the arriving pulse will give some indication of the effects of water column dynamics independent of surface scattering dynamics, since the surface bounce will not have arrived until after this time.

TABLE 1. Ray Travel Time

Ray path	arrival angle (deg)	arrival time (ms)
direct	-1.318	45.496
first bottom bounce	-6.202	45.752
first surface bounce	8.186	45.952

Figure 9 shows waterfall plots of the leading 500 μsec (3 cycles) of the time signal for 400 pulses received on a single hydrophone near the center of the horizontal array at a range of 70 m. These pulses have been rectified to show only the positive peaks of the linear FM received wave train. Fig. 4(a). was from a calm day, and Fig. 4(b) a windy day (maximum recorded winds 20 m/s). On the calm day, very little fluctuation of arrival time is evident. Contrast this with the windy day, where there is a great deal of both temporal and amplitude fluctuation in the arriving pulses.

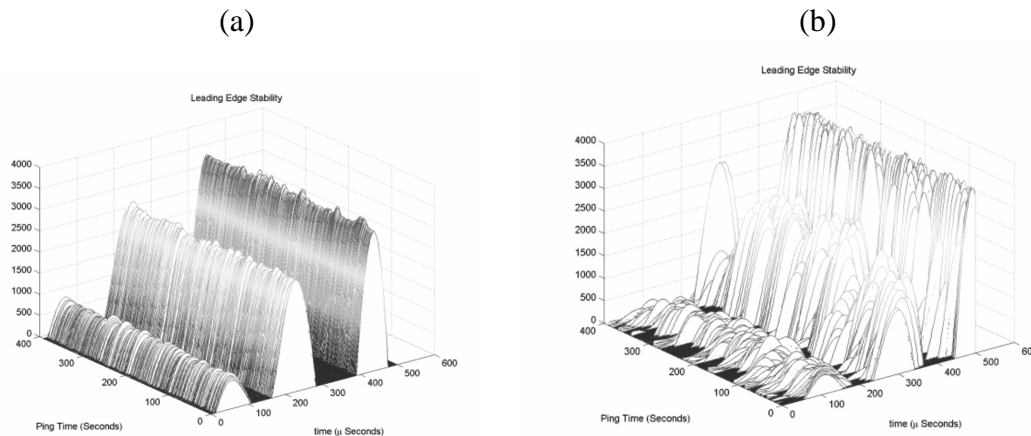


FIGURE 9. Waterfall plot of the leading edge of received pulses Vs time

These results are summarized in Fig 10, which shows the probability density functions for the arrival times for the calm and windy days. On the calm day, the time of arrival was most consistently measured to be 47.06 ms, with a standard deviation of 1 μsec (the sampling period). On the rough day, a spread of nearly 150 μsec was measured, suggesting a nearly 4.7 m/s fluctuation in average sound speed. The nearly 0.04 ms offset in the mean arrival time for each run is believed to be caused by variation in soundspeed. It is conjectured that this was due to bubble effects caused by the breaking waves and whitecaps which occurred during the rough day; a result that is in agreement with [3].

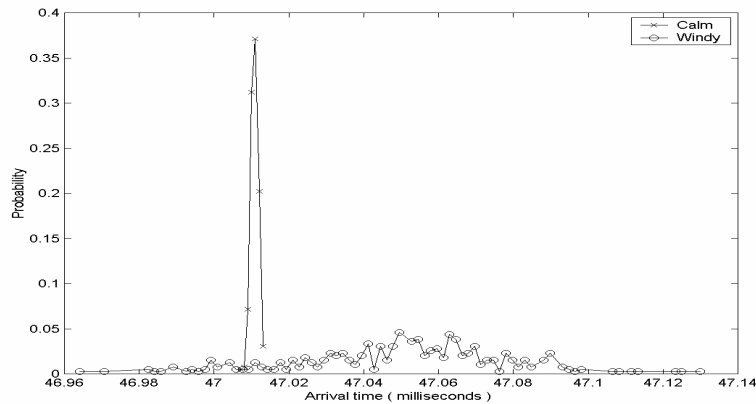


FIGURE10. Distribution of arrival times for a calm and a windy day.

SUMMARY

During these experiments the mean of the measured broadband temporal coherence for the time scales examined was seen to be 0.47 and was relatively stationary as a function of temporal delay. This result is in agreement with [1] for the Rayleigh noise case. There was a fluctuation about the mean of approximately $\pm 10\%$. The time of arrivals showed a significant difference between the calm day and the stormy day. While there was very little arrival fluctuation evident on the calm day, there was still significant de-correlation. This would suggest that on calm days, the effect of water column sound speed microstructure dynamics is small compared to surface scattering multipath effects, a result consistent with [4]. Earlier work [5] has reported higher values of coherence for a similar environment. However, comparison of these results with those presented here is not possible since we have not matched filtered our data prior to calculating coherence. Subsequent work will address these issues

ACKNOWLEDGMENTS

This work was supported by the Office of Naval Research, technical management by the Naval Research Laboratory, under program element 0602435N.

REFERENCES

1. Meredith, R., et al., "Panama City 2003 Acoustic Coherence Experiments: Environmental Characterization," in *Proceedings of the High-Frequency Ocean Acoustics Conference, 2004*.
2. Stanic, S., et al., "Panama City 2003 Broadband Shallow-Water Acoustic Coherence Experiments," in *Proceedings of the High-Frequency Ocean Acoustics Conference, 2004*.
3. Chotiros, N. P., et al, "Acoustic backscattering at low grazing angles from the ocean bottom. Part II. Statistical characteristics of bottom backscatter at a shallow water site," in *J. Acoust. Soc. Am.*, 77(3), March 1985.
4. Goodman, R. R., et al, "Observations of High-Frequency Sound Propagation in Shallow Water with Bubbles Due to Storm and Surf.," in *IEEE Journal of Oceanic Engineering*, Vol 25, No.4, October, 2000.
5. Badiy, M., et al, "Signal Variability in Shallow-Water Sound Channels.," in *IEEE Journal of Oceanic Engineering*, Vol 25, No.4, October, 2000.